

PAPER • OPEN ACCESS

Nuclear effects in (anti)neutrino charge-current quasielastic scattering at MINER ν A kinematics

To cite this article: M.V. Ivanov *et al* 2018 *J. Phys.: Conf. Ser.* **1023** 012028

View the [article online](#) for updates and enhancements.

You may also like

- [Ordering and dynamics of the central tetrahedron in the 1/1 \$Zn_{12}Sc\$ periodic approximant to quasicrystal](#)
Holger Euchner, Tsunetomo Yamada, Helmut Schober et al.
- [Tetrahedron dynamics in the icosahedral quasicrystals i-ZnMgSc and i-ZnAgSc and the cubic 1/1-approximant \$Zn_{12}Sc\$](#)
H Euchner, T Yamada, S Rols et al.
- [Neutron spectroscopy and strongly correlated electrons: a view from the inside](#)
P A Alekseev



ECS The Electrochemical Society
Advancing solid state & electrochemical science & technology


242nd ECS Meeting

Oct 9 – 13, 2022 • Atlanta, GA, US

Presenting more than 2,400 technical abstracts in 50 symposia

 **ECS Plenary Lecture** featuring **M. Stanley Whittingham**, Binghamton University Nobel Laureate – 2019 Nobel Prize in Chemistry

 **Register now!**



Nuclear effects in (anti)neutrino charge-current quasielastic scattering at MINER ν A kinematics

M.V. Ivanov¹, A.N. Antonov¹, G.D. Megias², R. González-Jiménez³, M.B. Barbaro⁴, J.A. Caballero², T.W. Donnelly⁵, and J.M. Udías⁶

¹ Institute for Nuclear Research and Nuclear Energy, Bulgarian Academy of Sciences, Sofia 1784, Bulgaria

² Departamento de Física Atómica, Molecular y Nuclear, Universidad de Sevilla, 41080 Sevilla, Spain

³ Department of Physics and Astronomy, Ghent University, Proeftuinstraat 86, B-9000 Gent, Belgium

⁴ Dipartimento di Fisica, Università di Torino and INFN, Sezione di Torino, Via P. Giuria 1, 10125 Torino, Italy

⁵ Center for Theoretical Physics, Laboratory for Nuclear Science and Department of Physics, Massachusetts Institute of Technology, Cambridge, Massachusetts 02139, USA

⁶ Grupo de Física Nuclear, Departamento de Física Atómica, Molecular y Nuclear, Facultad de Ciencias Físicas, Universidad Complutense de Madrid, Madrid E-28040, Spain

E-mail: martin@inrne.bas.bg

Abstract. We compare the characteristics of the charged-current quasielastic (anti)neutrino scattering obtained in two different nuclear models, the phenomenological SuperScaling Approximation and the model using a realistic spectral function $S(p, \mathcal{E})$ that gives a scaling function in accordance with the (e, e') scattering data, with the recent data published by the MiniBooNE, MINER ν A, and NOMAD collaborations. The spectral function accounts for the nucleon-nucleon (NN) correlations by using natural orbitals from the Jastrow correlation method and has a realistic energy dependence. Both models provide a good description of the MINER ν A and NOMAD data without the need of an *ad hoc* increase of the value of the mass parameter in the axial-vector dipole form factor. The models considered in this work, based on the the impulse approximation (IA), underpredict the MiniBooNE data for the flux-averaged charged-current quasielastic $\nu_\mu(\bar{\nu}_\mu) + {}^{12}\text{C}$ differential cross section per nucleon and the total cross sections, although the shape of the cross sections is represented by the approaches. The discrepancy is most likely due to missing of the effects beyond the IA, *e.g.*, those of the $2p$ - $2h$ meson exchange currents that have contribution in the *transverse responses*.

1. Introduction

The MINER ν A Collaboration has recently measured differential cross sections for neutrino and antineutrino charged-current quasielastic (CCQE) scattering on a hydrocarbon target [1, 2]. “Quasielastic” events are defined, in this case, as containing no mesons in the final state. The beam energy goes from 1.5 to 10 GeV and is peaked at $E_\nu \sim 3.5$ GeV. At lower energies $E_\nu \sim 0.8$ GeV the MiniBooNE experiment has reported [3, 4] CCQE cross sections that are higher than most theoretical predictions based on the impulse approximation (IA), leading to the suggestion that non-QE processes induced by two-body currents may play a significant role in this energy domain [5–8]. These effects have sometimes been simulated, in the Relativistic Fermi



Gas (RFG) framework, by a value of the nucleon axial-vector dipole mass $M_A = 1.35$ GeV [3, 4], which is significantly larger than the standard value $M_A = 1.03$ GeV extracted from neutrino-deuterium quasielastic scattering. On the other hand, higher-energy data from the NOMAD experiment ($E_\nu \sim 3 - 100$ GeV) [9] are well accounted for by IA models [10]. The MINER ν A experiment is situated in between these two energy regions and its interpretation can therefore provide valuable information on the longstanding problem of assessing the role of correlations and meson exchange currents (MEC) in the nuclear dynamics [11–13].

In this paper we present results corresponding to two different nuclear models: the SuSA (SuperScaling Approximation) and the model using a realistic spectral function $S(p, \mathcal{E})$. Both have been extensively tested against existing QE electron scattering data over a wide energy range. The detailed description of these models can be found in our previous work (see, *e.g.*, [14] and [15–17]). Here we just summarize their main features.

2. Theoretical Scheme and Results

SuSA [14] is based on the idea of using electron scattering data to predict CC neutrino cross sections: a phenomenological “superscaling function” $f(\psi)$, depending only on one “scaling variable” $\psi(q, \omega)$ and embodying the essential nuclear dynamics, can be extracted from QE longitudinal (e, e') data within a fully relativistic framework. This function is then multiplied by the appropriate charge-changing $N \rightarrow N$ ($n \rightarrow p$ for neutrino and $p \rightarrow n$ for antineutrino scattering) weak interaction cross sections to obtain the various response functions that contribute to the inclusive neutrino-nucleus cross section [18]. On the one hand, the model gives a good representation of the purely nucleonic contributions to the existing QE electron scattering data, to the extent that the quasielastic scattering can be isolated. On the other hand, it does not account for the inelastic scattering and MEC which are mainly seen in the transverse channel. For the former, the SuSA approach has been successfully extended to higher energies into the non-QE regime where inelastic contributions dominate [19]. The latter have been modeled using extensions of the RFG for two-body operators and typically cause 10 – 20% scaling violations.

The second model we consider is the model using a realistic spectral function $S(p, \mathcal{E})$ that gives a scaling function in accordance with the (e, e') scattering data [15–17]. Within the PWIA (see, *e.g.*, [15, 20] and details therein) the differential cross section for the ($e, e'N$) process factorizes in the form

$$\left[\frac{d\sigma}{de'd\Omega'dp_N d\Omega_N} \right]_{(e,e'N)}^{PWIA} = K \sigma^{eN}(q, \omega; p, \mathcal{E}, \phi_N) S(p, \mathcal{E}), \quad (1)$$

where σ^{eN} is the electron-nucleon cross section for a moving off-shell nucleon, K is a kinematical factor and $S(p, \mathcal{E})$ is the spectral function giving the probability to find a nucleon of certain momentum and energy in the nucleus. In Eq. (1): p is the missing momentum and \mathcal{E} is the excitation energy of the residual system. The scaling function can be represented in the form:

$$F(q, \omega) \cong \frac{[d\sigma/de'd\Omega']_{(e,e')}}{\bar{\sigma}^{eN}(q, \omega; p = |y|, \mathcal{E} = 0)}, \quad (2)$$

where the electron-single nucleon cross section $\bar{\sigma}^{eN}$ is taken at $p = |y|$, y being the smallest possible value of p in electron-nucleus scattering for the smallest possible value of the excitation energy ($\mathcal{E} = 0$). The theoretical concept of superscaling has been introduced within the relativistic Fermi gas (RFG) model [21, 22]. In the RFG model the scaling function $f_{\text{RFG}}(\psi') = k_F \cdot F$ has the form [23]:

$$f_{\text{RFG}}(\psi') \simeq \frac{3}{4} (1 - \psi'^2) \theta(1 - \psi'^2). \quad (3)$$

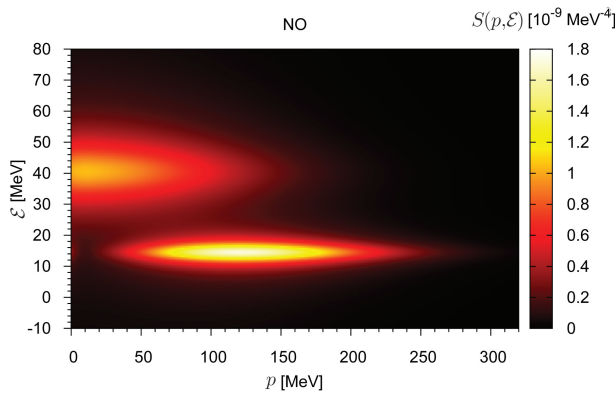


Figure 1. The ^{12}C realistic spectral function $S(p, \mathcal{E})$, which is constructed using natural orbital single-particle momentum distributions from the Jastrow correlation method and Lorentzian function for the energy dependence.

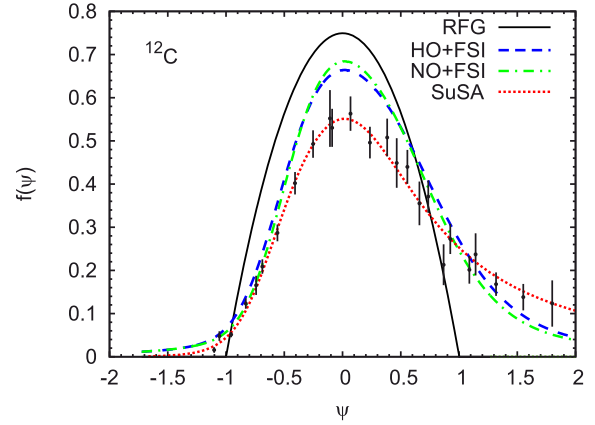


Figure 2. Results for the scaling function $f(\psi)$ for ^{12}C obtained using HO+FSI and NO+FSI approaches are compared with the RFG and SuSA results, as well as with the longitudinal experimental data.

As pointed out in [23], however, the actual dynamical physical reason of the superscaling is more complex than that provided by the RFG model.

In Ref. [15] more information about the spectral function was extracted within PWIA from the experimentally known scaling function. It contains effects beyond the mean-field approximation leading to a realistic energy dependence and accounts for short-range NN correlations. It is written in the form:

$$S(p, \mathcal{E}) = \sum_i 2(2j_i + 1)n_i(p)L_{\Gamma_i}(\mathcal{E} - \mathcal{E}_i), \quad (4)$$

where the Lorentzian function is used:

$$L_{\Gamma_i}(\mathcal{E} - \mathcal{E}_i) = \frac{1}{\pi} \frac{\Gamma_i/2}{(\mathcal{E} - \mathcal{E}_i)^2 + (\Gamma_i/2)^2} \quad (5)$$

with Γ_i being the width of a given s.p. hole state. In the calculations we used the values $\Gamma_{1p} = 6$ MeV and $\Gamma_{1s} = 20$ MeV, which are fixed to the experimental widths of the 1p and 1s states in ^{12}C [24]. In Eq. (4) the s.p. momentum distributions $n_i(p)$ were taken firstly to correspond to harmonic-oscillator (HO) shell-model s.p. wave functions, and second, to natural orbitals (NOs) s.p. wave functions $\varphi_\alpha(\mathbf{r})$ defined in [25] as the complete orthonormal set of s.p. wave functions that diagonalize the one-body density matrix $\rho(\mathbf{r}, \mathbf{r}')$:

$$\rho(\mathbf{r}, \mathbf{r}') = \sum_\alpha N_\alpha \varphi_\alpha^*(\mathbf{r}) \varphi_\alpha(\mathbf{r}'), \quad (6)$$

where the eigenvalues N_α ($0 \leq N_\alpha \leq 1$, $\sum_\alpha N_\alpha = A$) are the natural occupation numbers. In [15] we used $\rho(\mathbf{r}, \mathbf{r}')$ obtained within the lowest-order approximation of the Jastrow correlation methods [26]. The realistic spectral function $S(p, \mathcal{E})$ is presented in figure 1, where the two shells 1p and 1s are clearly visible.

For accounting for the FSI we follow the approach given in Ref. [27] concerning two types of FSI effects, the Pauli blocking and the interaction of the struck nucleon with the spectator system by means of the time-independent optical potential (OP) $U = V - iW$. The latter can

be accounted for [28] by the replacing in the PWIA expression for the inclusive electron-nucleus scattering cross section

$$\frac{d\sigma_t}{d\omega d|\mathbf{q}|} = 2\pi\alpha^2 \frac{|\mathbf{q}|}{E_k^2} \int dE d^3p \frac{S_t(\mathbf{p}, E)}{E_{\mathbf{p}} E_{\mathbf{p}'}} \delta(\omega + M - E - E_{\mathbf{p}'}) L_{\mu\nu}^{\text{em}} H_{\text{em},t}^{\mu\nu} \quad (7)$$

the energy-conserving delta-function by

$$\delta(\omega + M - E - E_{\mathbf{p}'}) \rightarrow \frac{W/\pi}{W^2 + [\omega + M - E - E_{\mathbf{p}'} - V]^2}. \quad (8)$$

In Eq. (7) the index t denotes the nucleon isospin, $L_{\mu\nu}^{\text{em}}$ and $H_{\text{em},t}^{\mu\nu}$ are the leptonic and hadronic tensors, respectively, and $S_t(\mathbf{p}, E)$ is the proton (neutron) spectral function. The real (V) and imaginary (W) parts of the OP in (7) and (8) are obtained in Ref. [29] from the Dirac OP.

The CC (anti)neutrino cross section in the target laboratory frame is given in the form (see for details [14, 30])

$$\left[\frac{d^2\sigma}{d\Omega dk'} \right]_{\chi} \equiv \sigma_0 \mathcal{F}_{\chi}^2, \quad (9)$$

where $\chi = +$ for neutrino-induced reaction *e.g.*, $\nu_{\ell} + n \rightarrow \ell^{-} + p$, where $\ell = e, \mu, \tau$ and $\chi = -$ for antineutrino-induced reactions (*e.g.*, $\bar{\nu}_{\ell} + p \rightarrow \ell^{+} + n$). The quantity \mathcal{F}_{χ}^2 in (9) depends on the nuclear structure and is presented [14] as a generalized Rosenbluth decomposition containing leptonic factors and five nuclear response functions, namely charge-charge (CC), charge-longitudinal (CL), longitudinal-longitudinal (LL), vector-transverse (T) and axial-transverse (T') expressed by the nuclear tensor and the scaling function.

To obtain the scaling function we use the spectral function $S(p, \mathcal{E})$ from (4) with $n_i(p)$ corresponding to HO or NOs s.p. wave functions, and the Lorentzian function (5). We calculate the electron- ^{12}C cross section by using Eqs. (7) and (8) and the scaling function $F(q, \omega)$ within the PWIA from Eq. (2). By multiplying $F(q, \omega)$ by k_F the scaling function $f(\psi')$ is obtained. In this way the results (figure 2) for the HO+FSI (dashed line) and NO+FSI (dash-dotted line) are obtained. As a reference are shown also the scaling functions in the cases of SuSA (dotted line) and RFG (solid line). The accounting for FSI leads to a small asymmetry of the scaling function. Also, we found that the asymmetry in the scaling function gets larger by using the Lorentzian function [Eq. (5)] for the energy dependence of the spectral function than by using the Gaussian function [15–17].

The results for the total cross sections obtained in [16] within the HO+FSI and NO+FSI are given in figure 3 and compared with the SuSA and RFG results and the MiniBooNE [3, 4] and NOMAD [9] data (up to 100 GeV). All models give results that agree with the NOMAD data but underpredict the MiniBooNE ones, more seriously in the ν_{μ} than in $\bar{\nu}_{\mu}$ cases. The discrepancy with the MiniBooNE data (at energies < 1 GeV) is most likely due to missing effects beyond the IA, *e.g.* those of the 2p-2h excitations that have contributions in the transverse responses. This concerns also the similar disagreement that appears when the phenomenological scaling function in SuSA is used. The latter, being extracted from the (e, e') data is a purely longitudinal QE response and thus is nearly insensitive to 2p-2h MEC contributions.

In figure 4 we display the flux-folded differential cross section $d\sigma/dQ_{\text{QE}}^2$ for both neutrino (left panel) and antineutrino (right panel) scattering off a hydrocarbon (CH) target as a function of the reconstructed four-momentum transfer squared (Q_{QE}^2), that is obtained in the same way as for the experiment, assuming an initial state nucleon at rest with a constant binding energy, E_b , set to 34 MeV (30 MeV) in the neutrino (antineutrino) case. The cross sections are folded with the MINER ν A ν_{μ} and $\bar{\nu}_{\mu}$ fluxes [1, 2], and the nucleon's axial mass has the standard value $M_A = 1.03$ GeV. We observe that RFG, SuSA, HO+FSI and NO+FSI approaches yield

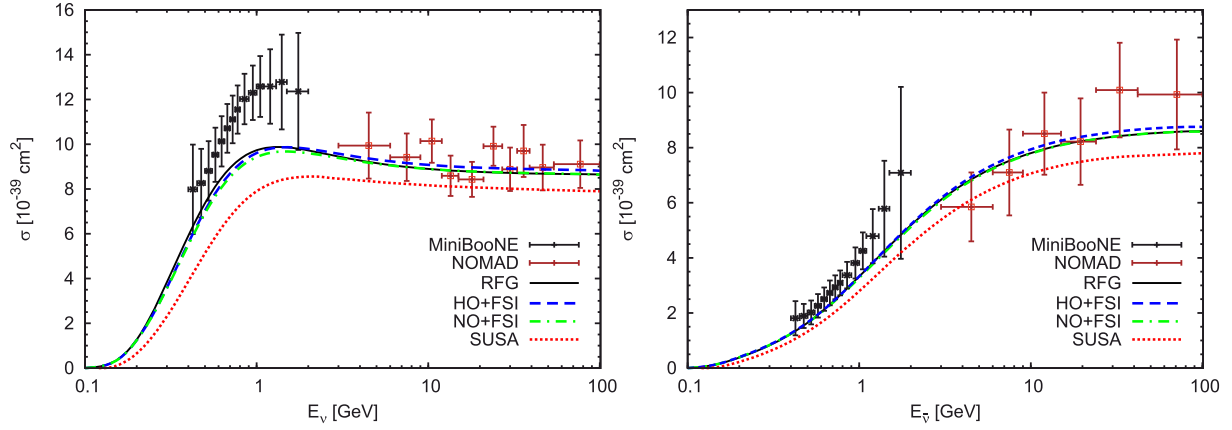


Figure 3. (left panel) CCQE $\nu_\mu + {}^{12}\text{C}$ total cross sections per nucleon displayed versus neutrino energy E_ν evaluated using the RFG, HO+FSI, NO+FSI, and SuSA approaches with the standard value of the axial-vector dipole mass $M_A = 1.03 \text{ GeV}/c^2$ are compared with the MiniBooNE [3, 4] and NOMAD [9] experimental data; (right panel) CCQE $\bar{\nu}_\mu + {}^{12}\text{C}$ total cross section.

predictions in excellent agreement with the experimental data, leaving not much space for large effects of 2p-2h contributions. HO+FSI and NO+FSI results are higher than the SuSA ones and lie closer to the RFG results. In the RFG calculation, we use the formalism of [21], assuming a Fermi momentum of 228 MeV/c and an energy shift of 20 MeV. This is not the same as the RFG modeling of GENIE [31] and NuWRO [32], which could explain the slight difference between our RFG results and the ones reported in [1, 2]. Note that the RFG model with the standard value of the axial mass (black-solid curve) also fits the data, being in very good agreement with the other approaches. Finally, the spread in the curves corresponding to the four models is less than 7% in the case of neutrinos and less than 5% in the case of antineutrinos. The theoretical results presented here include the whole energy range for the neutrino. The experimentalists implement several cuts on the phase space of the data, such as restricting the kinematics to contributions from neutrino energies below 10 GeV. The impact of such a cut on the results we present here is smaller than 0.2%, in the worst case. In the experimental analysis, several cuts were imposed to

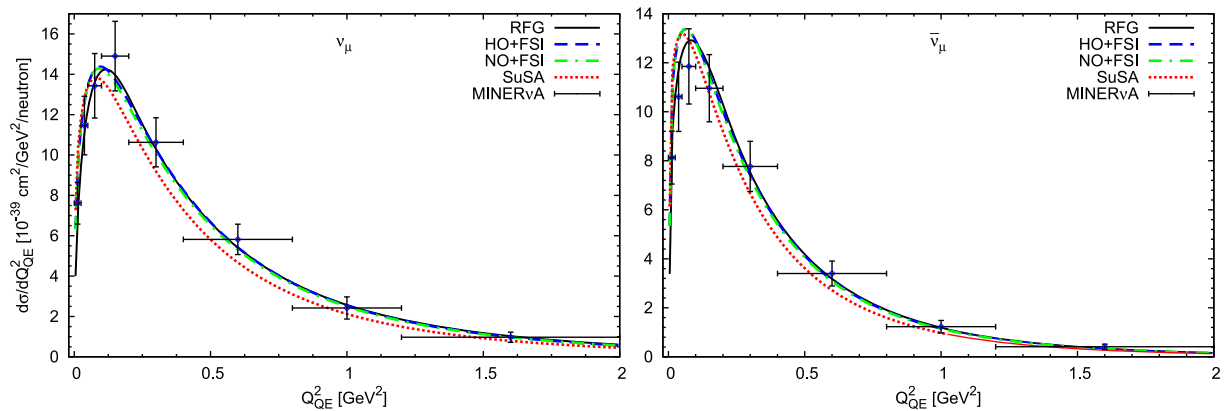


Figure 4. Flux-folded CCQE $\nu_\mu + {}^{12}\text{C}$ (left panel) and $\bar{\nu}_\mu + {}^{12}\text{C}$ (right panel) scattering cross section per target nucleon as a function of Q_{QE}^2 and evaluated in the SuSA, RFG, HO+FSI, and NO+FSI models; data [1, 2].

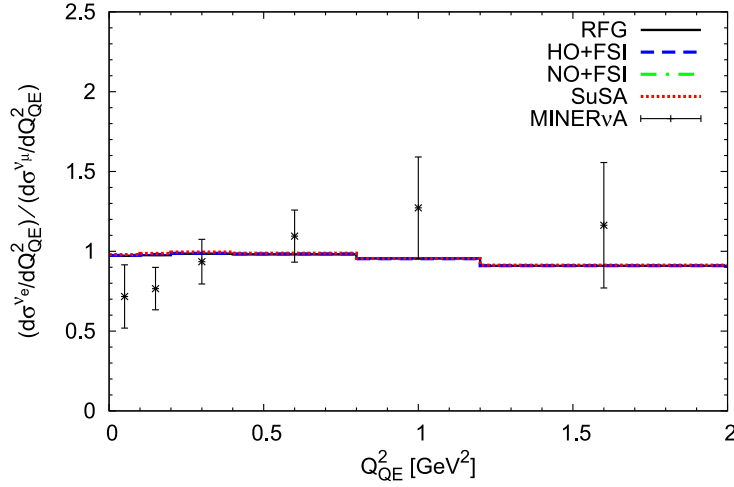


Figure 5. The ratio of the MINERνA ν_e CCQE differential cross section [34] as a function of Q_{QE}^2 to the analogous result from MINERνA for ν_μ [1].

the initial data sample to increase the ratio of true quasielastic events in the sample. The effect of these cuts has been incorporated into the efficiency factors of the experiment, and thus, the data have been corrected for them [33]. We apply no cuts to the theoretical results, as the data have been corrected for their effect.

For completeness, we present in the figure 5 the results corresponding the ratio of the MINERνA ν_e CCQE differential cross section [34] as a function of the reconstructed four-momentum Q_{QE}^2 to the analogous result from MINERνA for ν_μ [1]. The theoretical results for the ratio obtained within the RFG, HO+FSI, NO+FSI, and SuSA models almost coincide and are in good agreement with the data. For small values of the reconstructed four-momentum (first two bins) our results overpredict the data. It is important to note that the large error bars presented by the data make this particular analysis rather questionable.

3. Conclusions

- 1) The results with different spectral functions (HO and NO) give quite similar results (within 5–7%) for the CCQE cross sections, signaling that the process is not too sensitive to the specific treatment of the bound state.
- 2) The FSI leads to an increase of about 2% using spectral functions with HO and NO s.p. wave functions, almost independently of the neutrino energy.
- 3) All approaches based on IA underestimate MiniBooNE data for the flux-averaged CCQE ($\nu_\mu(\bar{\nu}_\mu) + {}^{12}\text{C}$) differential cross sections and the total cross section although the shape of the cross section is represented by NO+FSI and HO+FSI approaches. For $\bar{\nu}$ the agreement is much better.
- 4) All models give results that are compatible with the MinervA and NOMAD data. This points to the importance of the evaluation of non-impulsive contributions, like those associated to MEC and their evolution with energy. The 2p-2h contributions may be responsible for the observed discrepancy in our analyses. Similar disagreement is observed for the phenomenological scaling function of SuSA, that is *purely longitudinal* QE response and *2p-2h MEC should not contribute to it when properly extracted from QE electron scattering, but could contribute to QE neutrino scattering because of the axial current.*

Acknowledgments

This work was partially supported by the Bulgarian National Science Fund under Contracts No. DFNI-T02/19 and No. DFNI-E02/6.

References

- [1] Fiorentini G A *et al.* (MINERvA Collaboration) 2013 *Phys. Rev. Lett.* **111**(2) 022502
- [2] Fields L *et al.* (MINERvA Collaboration) 2013 *Phys. Rev. Lett.* **111**(2) 022501
- [3] Aguilar-Arevalo A A *et al.* (MiniBooNE Collaboration) 2010 *Phys. Rev. D* **81**(9) 092005
- [4] Aguilar-Arevalo A A *et al.* (MiniBooNE Collaboration) 2013 *Phys. Rev. D* **88**(3) 032001
- [5] Martini M, Ericson M, Chanfray G and Marteau J 2010 *Phys. Rev. C* **81**(4) 045502
- [6] Amaro J, Barbaro M, Caballero J, Donnelly T and Williamson C 2011 *Physics Letters B* **696** 151–155
- [7] Amaro J E, Barbaro M B, Caballero J A and Donnelly T W 2012 *Phys. Rev. Lett.* **108**(15) 152501
- [8] Nieves J, Simo I R and Vacas M V 2012 *Physics Letters B* **707** 72–75
- [9] Lyubushkin V *et al.* (NOMAD Collaboration) 2009 *Eur. Phys. J. C* **63** 355–381
- [10] Megias G, Amaro J, Barbaro M, Caballero J and Donnelly T 2013 *Physics Letters B* **725** 170–174
- [11] Donnelly T, van Orden J, de Forest T and Hermans W 1978 *Physics Letters B* **76** 393–396
- [12] De Pace A, Nardi M, Alberico W M, Donnelly T W and Molinari A 2003 *Nucl. Phys. A* **726** 303
- [13] Amaro J E, Maieron C, Barbaro M B, Caballero J A and Donnelly T W 2010 *Phys. Rev. C* **82**(4) 044601
- [14] Amaro J E, Barbaro M B, Caballero J A, Donnelly T W, Molinari A and Sick I 2005 *Phys. Rev. C* **71** 015501
- [15] Antonov A N *et al.* 2011 *Phys. Rev. C* **83**(4) 045504
- [16] Ivanov M V *et al.* 2014 *Phys. Rev. C* **89**(1) 014607
- [17] Ivanov M V *et al.* 2015 *Phys. Rev. C* **91**(3) 034607
- [18] Megias G D *et al.* 2014 *Phys. Rev. D* **89**(9) 093002
- [19] Maieron C *et al.* 2009 *Phys. Rev. C* **80** 035504
- [20] Caballero J A, Barbaro M B, Antonov A N, Ivanov M V and Donnelly T W 2010 *Phys. Rev. C* **81**(5) 055502
- [21] Alberico W M *et al.* 1988 *Phys. Rev. C* **38** 1801
- [22] Barbaro M B, Cenni R, Pace A D, Donnelly T W and Molinari A 1998 *Nucl. Phys. A* **643** 137
- [23] Donnelly T W and Sick I 1999 *Phys. Rev. C* **60** 065502
- [24] Dutta D 1999 *The ($e, e'p$) Reaction Mechanism in the Quasi-Elastic Region* Ph.D. thesis Northwestern University
- [25] Löwdin P O 1955 *Phys. Rev.* **97**(6) 1474–1489
- [26] Stoitsov M V, Antonov A N and Dimitrova S S 1993 *Phys. Rev. C* **48**(1) 74–86
- [27] Ankowski A M and Sobczyk J T 2008 *Phys. Rev. C* **77**(4) 044311
- [28] Horikawa Y, Lenz F and Mukhopadhyay N C 1980 *Phys. Rev. C* **22**(4) 1680–1695
- [29] Cooper E D, Hama S and Clark B C 2009 *Phys. Rev. C* **80**(3) 034605
- [30] Antonov A N *et al.* 2006 *Phys. Rev. C* **74**(5) 054603
- [31] Andreopoulos C 2009 *Acta Phys. Pol. B* **40**(9) 2461
- [32] Golan T, Juszczak C and Sobczyk J T 2012 *Phys. Rev. C* **86**(1) 015505
- [33] Chvojka J 2012 *Anti-Neutrino Charged Current Quasi-Elastic Scattering in MINERvA* Ph.D. thesis University of Rochester
- [34] Wolcott J *et al.* (MINERvA Collaboration) 2016 *Phys. Rev. Lett.* **116**(8) 081802